2016-12

Modeling of plutonium ionization probabilities for use in nuclear forensic analysis by resonance ionization mass spectrometry

Hutchinson, Steven F.

Monterey, California: Naval Postgraduate School

NAVAL POSTGRADUATE SCHOOL

MONTEREY, CALIFORNIA

THESIS

MODELING OF PLUTONIUM IONIZATION PROBABILITIES FOR USE IN NUCLEAR FORENSIC ANALYSIS BY RESONANCE IONIZATION MASS SPECTROMETRY

by

Steven F. Hutchinson

December 2016

Thesis Advisor: Craig F. Smith
Co-Advisor: Brett Isselhardt

THIS PAGE INTENTIONALLY LEFT BLANK

REPORT DOCUMENTATION PAGE			*Form Approved OMB No. 0704-0188*

1. AGENCY USE ONLY *(Leave blank)*	**2. REPORT DATE** December 2016	**3. REPORT TYPE AND DATES COVERED** Master's thesis

4. TITLE AND SUBTITLE MODELING OF PLUTONIUM IONIZATION PROBABILITIES FOR USE IN NUCLEAR FORENSIC ANALYSIS BY RESONANCE IONIZATION MASS SPECTROMETRY	**5. FUNDING NUMBERS**
6. AUTHOR(S) Steven F. Hutchinson	
7. PERFORMING ORGANIZATION NAME(S) AND ADDRESS(ES) Naval Postgraduate School Monterey, CA 93943-5000	**8. PERFORMING ORGANIZATION REPORT NUMBER**
9. SPONSORING /MONITORING AGENCY NAME(S) AND ADDRESS(ES) N/A	**10. SPONSORING / MONITORING AGENCY REPORT NUMBER**

11. SUPPLEMENTARY NOTES The views expressed in this thesis are those of the author and do not reflect the official policy or position of the Department of Defense or the U.S. Government. IRB number ____N/A____.

12a. DISTRIBUTION / AVAILABILITY STATEMENT Approved for public release. Distribution is unlimited.	**12b. DISTRIBUTION CODE** A

13. ABSTRACT (maximum 200 words)

Recent advancements in nuclear forensics have enabled the use of lasers via resonance ionization mass spectrometry (RIMS) to determine the isotopic composition ratios of U-235 and U-238. These technological advancements aid the field of nuclear forensics by establishing a known database and modeling approach for quantifying uranium isotope ionization probabilities. In order to further enhance the data and modeling capability necessary for nuclear forensics, numerical simulations must be analyzed and compared to experimental results conducted at Lawrence Livermore National Laboratory (LLNL).

This research extends previous RIMS data simulation analysis conducted at Naval Postgraduate School (NPS) and LLNL. The modeling framework collaborates with the experimental data to empirically derive the ionization cross sections for plutonium, furthering the confidence in the use of RIMS for nuclear forensic analysis. By implementing the experimental data into the modeling framework, we are able to provide the Department of Defense a more rapid nuclear forensics process.

14. SUBJECT TERMS plutonium, RIMS, nuclear forensics, laser ionization, resonance laser	**15. NUMBER OF PAGES** 61
	16. PRICE CODE

17. SECURITY CLASSIFICATION OF REPORT	**18. SECURITY CLASSIFICATION OF THIS PAGE**	**19. SECURITY CLASSIFICATION OF ABSTRACT**	**20. LIMITATION OF ABSTRACT**
Unclassified	Unclassified	Unclassified	UU

NSN 7540-01-280-5500 Standard Form 298 (Rev. 2-89) Prescribed by ANSI Std. 239-18

THIS PAGE INTENTIONALLY LEFT BLANK

Approved for public release. Distribution is unlimited.

MODELING OF PLUTONIUM IONIZATION PROBABILITIES FOR USE IN NUCLEAR FORENSIC ANALYSIS BY RESONANCE IONIZATION MASS SPECTROMETRY

Steven F. Hutchinson
Lieutenant, United States Navy
B.S., Oregon State University, 2010

Submitted in partial fulfillment of the
requirements for the degree of

MASTER OF SCIENCE IN APPLIED PHYSICS

from the

NAVAL POSTGRADUATE SCHOOL
December 2016

Approved by: Craig F. Smith
Thesis Advisor

Brett Isselhardt, Lawrence Livermore National Laboratory
Co-Advisor

Kevin B. Smith
Chair, Department of Physics

THIS PAGE INTENTIONALLY LEFT BLANK

ABSTRACT

Recent advancements in nuclear forensics have enabled the use of lasers via resonance ionization mass spectrometry (RIMS) to determine the isotopic composition ratios of U-235 and U-238. These technological advancements aid the field of nuclear forensics by establishing a known database and modeling approach for quantifying uranium isotope ionization probabilities. In order to further enhance the data and modeling capability necessary for nuclear forensics, numerical simulations must be analyzed and compared to experimental results conducted at Lawrence Livermore National Laboratory (LLNL).

This research extends previous RIMS data simulation analysis conducted at Naval Postgraduate School (NPS) and LLNL. The modeling framework collaborates with the experimental data to empirically derive the ionization cross sections for plutonium, furthering the confidence in the use of RIMS for nuclear forensic analysis. By implementing the experimental data into the modeling framework, we are able to provide the Department of Defense a more rapid nuclear forensics process.

THIS PAGE INTENTIONALLY LEFT BLANK

TABLE OF CONTENTS

THIS PAGE INTENTIONALLY LEFT BLANK

LIST OF FIGURES

THIS PAGE INTENTIONALLY LEFT BLANK

LIST OF TABLES

THIS PAGE INTENTIONALLY LEFT BLANK

LIST OF ACRONYMS AND ABBREVIATIONS

AI	auto ionization
Am	americium
amu	atomic mass unit
cm	centimeter
FES	first excited state
FWHM	full width half maximum
Ga	gallium
ITU	Institute for Transuranium Elements
K	Kelvin
LION	Laser Ionization of Neutrals
LLNL	Lawrence Livermore National Laboratory
MeV	mega electron volt
mW	milli-watt
Np	neptunium
ns	nanosecond
pm	picometer
Pu	plutonium
RIMS	resonance ionization mass spectrometry
SEM	scanning electron microscopy
SES	second excited state
SIMS	secondary ionization mass spectrometry
TIMS	thermal ionization mass spectrometry
TNT	trinitrotoluene
U	uranium

THIS PAGE INTENTIONALLY LEFT BLANK

ACKNOWLEDGMENTS

It has been a long, complex journey to reach the achievement of becoming a Naval Postgraduate School graduate. I reflect back in amazement on how I was able to get to where I am today. It started as a young 17-year-old high school graduate, still trying to determine how I was going to get into college, to a successful United States Naval Officer with a master of science degree in applied physics.

Special thanks go to my parents for their support as I traversed my path in the U.S. Navy. They provided me with sound advice through my many years of service. Also, I would like to thank my love, Megan, for her strength and commitment to our growing family. At times this lifestyle we endured together has been difficult, but your love and kindness has kept the tremendous bond in our family strong.

Second, I would like to thank my thesis advisor, Dr. Craig Smith, for his wisdom and support through the educational process. Your advice did not go unnoticed, especially during the daunting stages of writing this thesis. Additionally, I would like to thank the Defense Threat Reduction Agency Basic Research Program for supporting this research. I also received help from Leslie Ann Alasagas of the Naval Academy. Her utmost dedication to this research and the RIMS project was much appreciated.

Finally, sincere gratitude to my co-advisor, Dr. Brett Isselhardt, for his immense subject expertise and patience as I strived to understand the quantum principles that governed this project. I greatly appreciate your travels to Monterey to assist me in fine-tuning the structure and details regarding the research.

THIS PAGE INTENTIONALLY LEFT BLANK

I. INTRODUCTION

For many decades, modern societies around the world have had a general and realistic idea of the potentially catastrophic impact the detonation of a nuclear device could have on a major metropolis. The immediate impacts could include large-scale loss of life, and the aftermath could lead to vast economic damage to the region of impact, in addition to physical damage to the surrounding infrastructures. The possibility of such potential damage was quickly realized by Enrico Fermi, only weeks after Hahn and Strassman wrote about their discovery of nuclear fission [1]. Fermi was standing in his office, looking out his window toward downtown Manhattan, and realized that a device fueled by a relatively small amount of highly enriched uranium could wipe out the borough [1].

After this discovery, many physicists were fascinated with nuclear fission as a potential usable energy source for generation of electrical power [1]. One neutron impacting a single nucleus of uranium-235 causes a fission energy release that yields, on average, 200 MeV [2]. This is an extraordinary amount of energy for a single reaction, and at the time was rightly considered a world-changing breakthrough in scientific research. Table 1 shows the energy breakdown of a typical fission reaction. It is interesting to note the byproducts from the reaction itself. The byproducts consist of a variety of fission product elements, gamma rays, neutrinos, beta particles and more neutrons. These neutrons have a spectrum of energies, and can lead to more fission reactions, thus creating the possibility of a chain reaction [2]. This possible chain reaction is the fundamental phenomenon that makes both the peaceful use of nuclear energy and the nuclear bomb possible.

Table 1. Distribution of Fission Energy. Adapted from [2].

Energy Form	MeV
Kinetic energy of fission fragments	165 +/- 5
Instantaneous gamma-ray energy	7 +/- 1
Kinetic energy of fission neutrons	5 +/- 0.5
Beta particles from fission products	7 +/- 1
Gamma rays from fission products	6 +/- 1
Neutrinos from fission products	10
Total energy per fission	**200 +/- 6**

A. NUCLEAR BOMB

In the midst of World War II, on August 13, 1942, the Manhattan Engineer District was established under the command of United States Army Colonel, James C. Marshall [3]. The establishment of the Manhattan Engineer District was to gain headway on the development of the world's first atomic weapon. Knowing the Germans experimented with nuclear fission three years prior, the Americans realized the need to speed up their efforts in producing a nuclear bomb that could achieve an explosive fission chain reaction in a relatively short amount of time [3].

The first atomic weapon produced and tested was a plutonium implosion-type bomb in the famous test named Trinity [3]. Trinity occurred ahead of schedule on July 16, 1945 in the New Mexico desert 210 miles south of Los Alamos (see Figure 1). Original predictions for first device called for it to be ready by August of that same year. The resultant explosion from Trinity was greater than any of the team's researchers predicted. The TNT equivalent yield from the test was estimated to be between 15,000 and 20,000 tons [3].

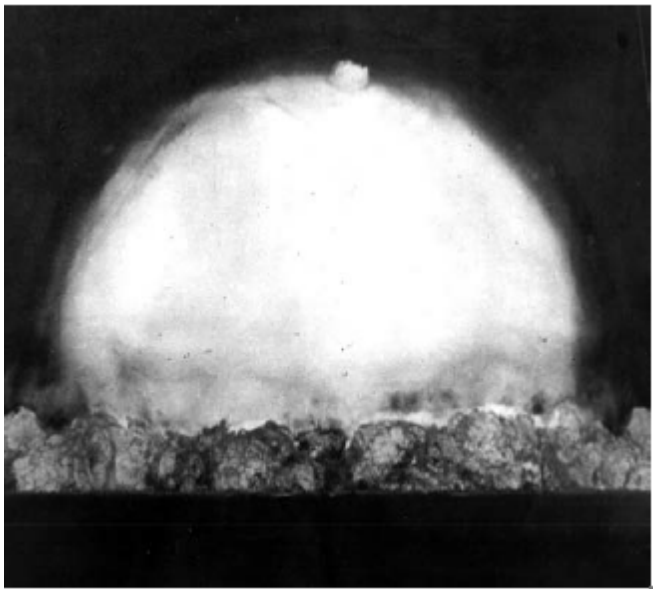

Figure 1. Trinity Test. Source: [1].

Two types of nuclear bomb devices were being developed during this time period, the gun-type device and the implosion device. The gun-type device used the concept of rapidly propelling a subcritical mass of highly enriched uranium into another subcritical mass of the same element. When these two subcritical masses collide, they form a supercritical mass. Criticality refers to the neutron population within the system. A critical system is one that can sustain a chain reaction in which there is a balance between the number of fission neutrons in one generation and in the succeeding generation. If more neutrons are produced in successive generations, the neutron population grows, and the system is considered supercritical [2]. Figure 2 shows a simple design of a gun-type nuclear bomb in which a highly supercritical condition is achieved by rapidly assembling two subcritical masses. This type of weapon was used by the United States on Hiroshima during World War II, and was referred to as “Little Boy” [3].

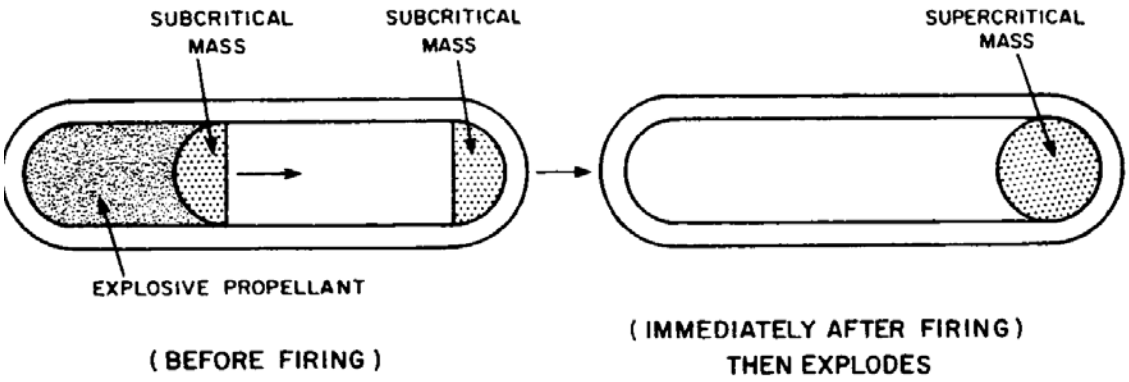

Figure 2. Gun-Type Nuclear Weapon Design. Source: [2].

The implosion nuclear device was the spherical-shaped design shown in Figure 3. This design used chemical explosives surrounding a subcritical mass of plutonium to implode its mass into a supercritical configuration [2]. The explosive yield of the chemical explosives is very small compared to the explosive yield of the supercritical fissile material. This was the same type of bomb first tested at the Trinity site in New Mexico, and then used by the United States over Nagasaki during World War II. This device was referred to as “Fat Man” [3].

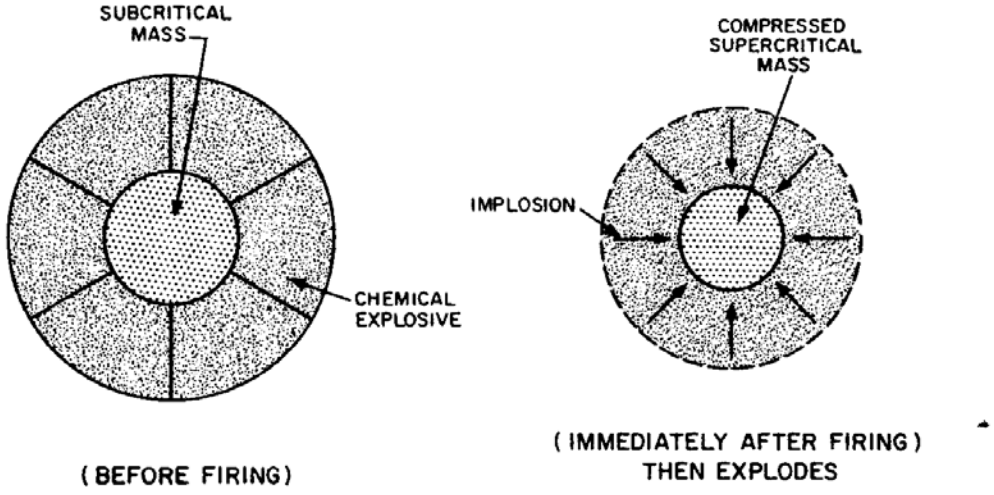

Figure 3. Principle of an Implosion-Type Device. Source: [2].

B. ROLE OF PLUTONIUM-239

The primary fissionable ingredient in the make-up of a fission nuclear bomb is either uranium-235 or plutonium-239. Either can be used to implement catastrophic damage to a vast region. The composition of the uranium in the earth's crust is about 0.7% uranium-235 and 99.3% uranium-238 [2]. The challenge of separating isotopes of the same element makes it very difficult to obtain pure uranium-235 with little to no uranium-238. Plutonium-239, on the other hand, is artificially produced in a nuclear reactor by conversion of the fertile uranium-238 [2]. These reactors usually have very soft (i.e., low energy) neutron spectra, and are operated in a way in which the fuel can continuously be reloaded. Heavy water and graphite moderated reactors are common types of reactors used to produce weapons grade plutonium [4]. Because of the production of plutonium (Pu) in commercial and government nuclear reactors, it is increasingly important that security measures are in place when storing, handling, and transferring spent nuclear fuel from such reactors.

C. NUCLEAR FORENSICS

Due to the nuclear device's massive destructive capabilities, it is quite apparent that the aftermath of its detonation is expected to be devastating. This makes it imperative that developed nations with access to advanced nuclear technology take explicit measures to ensure that nuclear materials potentially usable for weapons purposes remain in secure control, inaccessible to adversary countries or groups desiring such materials for malicious intent. Numerous cases of "nuclear smuggling" occurred in Europe just after the fall of the Soviet Union. This led to the development of a new form of criminal forensics, now known as nuclear forensics [4].

In March 1992, seized nuclear material was analyzed at the Institute for Transuranium Elements (ITU) by thermal ionization mass spectrometry (TIMS) in order to determine the isotopic composition of the material [4]. Determining the isotopic make-up and the chemical constituents of any seized materials can enable forensic experts to understand the origins of the material. This March 1992 seizure of nuclear material involved a uranium pellet intended for reactor fuel, and its isotopic composition was less

than the 90% ^{235}U enrichment required to be considered weapons-grade nuclear material [4].

There are many types of pre-detonation nuclear forensics methods available for microscopic analysis of the material composition. These spatially resolved techniques include secondary ionization mass spectrometry (SIMS) and scanning electron microscopy (SEM) which focus primarily on particle and powder analysis [4]. SEM can be coupled with electron dispersive X-ray to determine the elemental composition [4]. Collectively, these methods help enhance the big picture pertaining to the origins of a particular sample seized for forensic analysis. Resonance Ionization Mass Spectrometry (RIMS) provides for a more rapid analysis of the isotopic composition of a sample when compared to TIMS or other analytical techniques requiring sample dissolution and chemical purification prior to analysis [5].

Nuclear forensics is useful for tracking and identifying sources of smuggled nuclear material; however, it may also be used to determine a material's origin in analysis of post detonation debris from a nuclear detonation. Post detonation debris from a nuclear device can be sampled and analyzed through nuclear forensics to determine the material and chemical composition within the sample. This data can then be included in analysis by law enforcement and intelligence agencies to determine which country or terrorist group detonated the device. An expedient process in analysis for this situation is vital to provide answers to the President of the United States and prominent leaders in the surrounding region of the detonated nuclear device. The method in which the material is analyzed contributes directly to the duration of the forensics process. Discovering new methods for rapid analysis in nuclear forensics further enhances the field of study. Advancements in the equipment size, such as engineering the nuclear forensics equipment to allow for portable use, greatly reduces the duration of analysis by cutting down the time between sample collection and sample analysis at a laboratory facility.

RIMS uses a small sample of debris material and analyzes it through the use of selective laser excitation followed by mass spectrometry [5]. The sample is placed in an ultra-high vacuum chamber and a small portion of the sample is atomized into a neutral gaseous form through the use of ion sputtering [5]. The atomization of the material is

performed with a Ga^+-ion gun just prior to the three-pulsed laser ionization process [5]. The atomization process inherently injects into the chamber both neutral particles and charged particles in the gas phase above the sample surface. Secondary ion suppression is required to remove the charged particles prior to laser ionization [5]. A 4 kV voltage is applied to the chamber for approximately 300 ns just prior to the excitation/ionization laser pulses to remove unwanted ions from the chamber that may interfere with RIMS analysis [5]. Once a neutral cloud of debris is obtained, the three selective lasers will excite and ionize the selected element in the material and an acceleration voltage (~2 kV) will be applied to draw the selectively ionized charged particles into the time-of-flight spectrometer for analysis. The difference in arrival time at the detector is used to separate the isotopes of the selected element by mass.

D. SCOPE OF THE RESEARCH

Recent advancements in nuclear forensics have enabled the use of lasers via RIMS to determine the isotopic ratios of the various isotopes of uranium (U) [6]. These technological advancements aid the field of nuclear forensics by establishing a rapid tool for material characterization. Along with the development of RIMS techniques, a model has been produced to aid development, understand the sensitivity of the technique to variations in laser performance, and for quantifying uranium isotope ionization probabilities. These probabilities have been obtained empirically by matching numerical simulations and experimental results and integrating these insights into the simulation framework. In an attempt to further enhance the data and modeling capability necessary to continue developing RIMS for nuclear forensics, numerical simulations of plutonium (Pu) isotopes must be analyzed and compared to experimental results in this research conducted at Lawrence Livermore National Laboratory (LLNL) in the Laser Ionization of Neutrals (LION) facility. The resulting enhancement of the simulation capability to enable analysis of Pu isotopes in debris is a key objective of this research.

This research extends previous work [6], carried out at LLNL by Dr. Brett Isselhardt and at Naval Postgraduate School [7], in the RIMS project to enhance a modeling/simulation capability to predict the ionization probabilities and isotope ratios

for elements of interest in analysis of debris from a nuclear detonation. This previous work developed the framework for the simulation/modeling and was successfully completed with uranium. The successful analysis of uranium allows us to confidently pursue additional isotopes of interest, such as, in this case, plutonium. It allows projections to be made based on analysis using pre-existing key atomic data, and incorporates the capability to further refine and improve the fidelity of simulations by including the results of additional RIMS experiments.

Additionally, through the analysis of plutonium isotopes, this research enhances the modeling/simulation capability to use RIMS for Department of Defense applications involving the analysis of debris from a nuclear detonation by introducing the ability to analyze/predict ionization probabilities and the corresponding isotope ratios of Pu-239, Pu-240 and other isotopes of plutonium. By exploring the range of laser parameters used in RIMS at the LLNL-LION facility we can determine the relative ionization probabilities of plutonium and compare the data with a known computer simulation model. The results of the model will increase our understanding of the systematic variation possible during experiments, enabling greater confidence in the experiment results, and will help lead to more rapid nuclear forensic analysis and therefore more information available early in a forensic investigation.

E. OUTLINE

In Chapter II, I discuss the fundamental concepts of the resonance ionization process and the techniques used in time-of-flight mass spectrometry. Chapter III discusses the composition of the model, to include the essential parameters involved and the assumptions made in order to achieve the desired results. Chapter IV analyzes and compares the experimental results with the model using the cross sections obtained from the experimental analysis. The final chapter is the conclusion, which summarizes the analysis and includes recommendations for future research.

II. RIMS FUNDAMENTAL THEORY

Among the advantages of using RIMS for isotopic analysis is that it uses an inherently quick process that is highly element (and isotope) selective, thereby providing a low background, and a corresponding high sensitivity [8]. Using three pulsed laser beams the plutonium in the neutral gaseous cloud will be selectively ionized [5]. Each laser is tuned to resonantly excite a specific electronic transition, including the final step into an ionized state. Once the atoms are excited from the electronic ground state and ionized, the resulting ions of plutonium are accelerated by an electric field into the drift region of the mass spectrometer and focused onto an ion counter for detection by time of flight. The difference in time of flight through the spectrometer is then used to quantify the isotopes due to their differences in mass to charge ratio [8]. Figure 4 shows the variety of possible ionization schemes when using tunable lasers to excite neutral atoms.

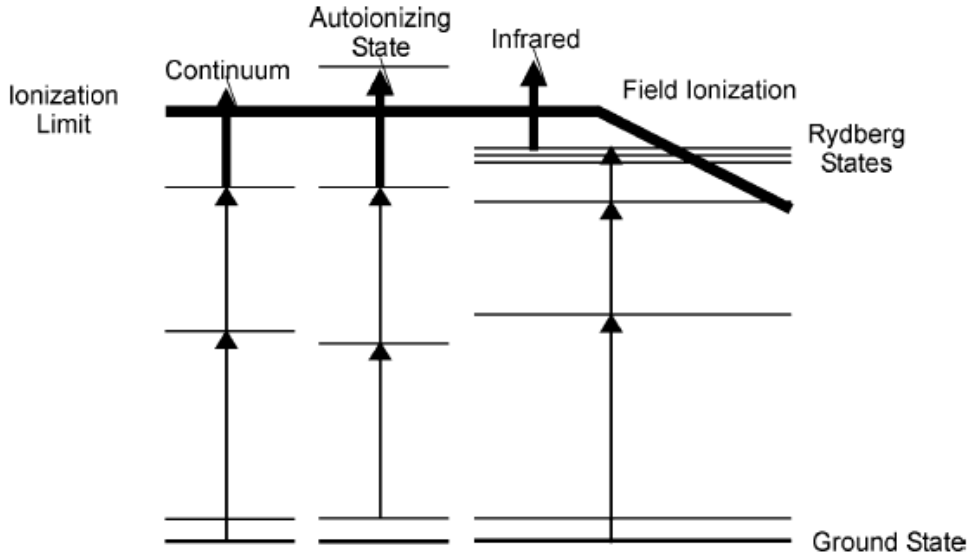

Figure 4. General Laser Induced Ionization Scheme. Source: [8].

The analysis of plutonium in the LLNL-LION facility implements a three-color, three-photon pulsed laser ionization process in order to resonantly excite and ionize plutonium, and maximize selectivity over other elements. The close alignment of the

energy levels of ^{239}Pu and ^{240}Pu in the ionization schemes are shown in Figure 5. The fundamental theory behind stimulated electronic transitions that is presented in this chapter is a direct synopsis of the work performed by Isselhardt, in [5] and [6]. Those references go into great detail on the quantum theory contained in laser ionization physics. This chapter primarily focuses on the transition between two energy states.

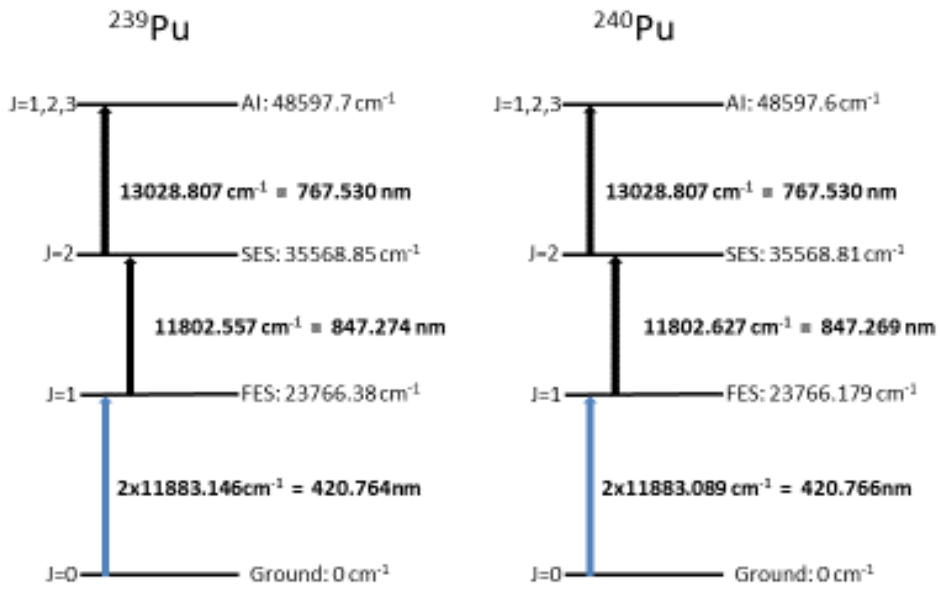

Figure 5. Pu-239 and Pu-240 Ionization Scheme. Adapted from [9].

A. ENERGY STATE TRANSITIONS

First we must examine the time dependent nature of two electronic states of an atom. Figure 6 shows the two-state atomic model to include the full-width-half-maximum (FWHM) or the uncertainty in energy Γ. Additionally, λ represents the spontaneous decay by photon emission of the upper state with an average lifetime $\tau = 1 / \lambda$. In [5], Isselhardt introduces the complex component of the energy as $\Gamma = \hbar / \tau$. However, when Γ is used as a function of angular frequency, it can be simplified to $1 / \tau$ [5].

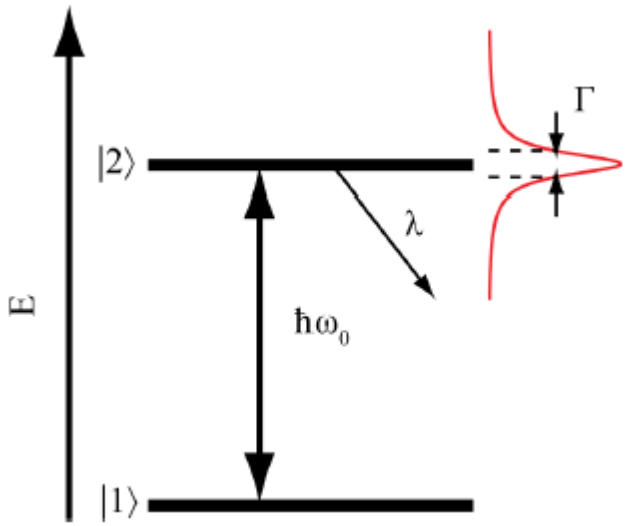

Figure 6. Energy Transition between Two States. Source: [5].

To understand the probability of a transition as a function of energy, it is important to relate these parameters as a function of energy. From [5], the normalized probability for finding a time-dependent state in energy is given as a Lorentzian distribution with FWHM of Γ centered about E_0:

$$P(E) = \frac{1}{2\pi} \frac{\Gamma}{(E + E_0)^2 + \left(\frac{\Gamma}{2}\right)^2}$$

B. STIMULATED EMISSION AND ABSORPTION

When a laser interacts with atoms and causes transitions between energy states, there are three possible outcomes to consider. The first two, stimulated emission and stimulated absorption, are the key components regarding a two state atomic system and have the same probability of occurrence [5]. The third possible outcome is spontaneous decay. As Isselhardt explains in [5], "consider a blackbody cavity of atomic vapor in thermodynamic equilibrium where the electromagnetic radiation density inside the cavity, regardless of the elemental composition of either cavity walls or the atomic vapor, is described by the Planck distribution,

$$u(\omega)\,\mathrm{d}\,\omega = \left(\frac{\hbar\omega^3 d\omega}{\pi^2 c^3}\right)\left[\frac{1}{\left(e^{\frac{\hbar\omega}{kT}}-1\right)}\right]$$

where $u(\omega)d\omega$ is the energy per unit volume." Relating this with the population between two energy states, state 1 and state 2 for a single photon transition is

$$\frac{N_2}{N_1} = \left(\frac{g_2}{g_1}\right)e^{\frac{-\hbar\omega_0}{kT}}$$

where g_i is the statistical weight of a state i, and is given via the total angular momentum of the state J_i ($g_i = 2J_i + 1$). Additionally, ω_o is resonant photon frequency for the transition between the two states [5]. From these equations, as expressed in [5], the probability per unit time of absorption, stimulated emission and spontaneous decay are given as follows:

$$\frac{dP_{abs}}{dt} = B_{12}\cdot u_{\omega}(\omega)$$
$$\frac{dP_{emit}}{dt} = B_{21}\cdot u_{\omega}(\omega)$$
$$\frac{dP_{decay}}{dt} = A_{21}$$

In the aforementioned equations A_{21}, B_{21}, and B_{12} are the Einstein coefficients for their respective equations [5]. Now for instance if state 2 can only decay into state 1 then A_{21} represents the inverse average lifetime of that state, essentially Γ_2 [5].

Developing equation relationships with the Einstein coefficients while maintaining an energy flow balance and thermal equilibrium will produce the cross section for absorption. Isselhardt derives these relationships in [5] and results in a cross section as a function of Γ_2

$$\sigma_a(\omega) = \frac{1}{4}\frac{g_2}{g_1}\lambda_0^2\Gamma_2 g(\omega)$$

C. ANGULAR MOMENTUM

Angular momentum is a principle factor when analyzing atoms at the quantum level. It is important to include the degeneracy of states via the statistical weight of the system, g_i as a function of angular momentum, where i is the number of energy states for that given isotope. These energy degeneracies for a given state will separate in the presence of an external field [5]. With no external field, the population for a given state (N_i) will relate to the summation of the degenerate states for that energy level. Recall that $g_i = 2J + 1$, thus the degeneracy of state is a function of the total angular moment [5]. If interactions are considered incoherent and under the assumption that all interactions are strongly saturated, the populations can be related to the degeneracy of states as shown in [5] as

$$\frac{N_2}{N_1} = \frac{g_2}{g_1}$$

D. DOPPLER BROADENING

Realistically atoms are moving in random directions, therefore, these atomic movements must be considered upon implementing our model. Isselhardt explains in [5], "in the non-relativistic limit, an atom with a resonance frequency ν_o traveling with a velocity V parallel to the propagation direction of the laser beam will experience a shift in frequency known as the Doppler shift." This Doppler shift is described by

$$\nu_D = \nu_0\left(1 + \frac{V}{c}\right)$$

where c is the speed of light. If the distribution of gaseous atoms is thermal, then the Maxwell-Boltzmann probability distribution will apply [5]. The frequency distribution about ν_o is a Gaussian distribution given in [5] by

$$D(\nu) = \frac{1}{\sqrt{2\pi\sigma}} e^{\frac{-(\nu-\nu_0)^2}{2\sigma^2}}$$

Thus, the Doppler width or FWHM of the distribution is given in [5] by

$$\Delta\nu_D = 2 \cdot \nu_0 \sqrt{\frac{2kT \cdot \ln 2}{mc^2}}$$

In terms of frequency and solving for the constants

$$\Delta\lambda_D = 7.16 \times 10^{-7} \cdot \lambda_0 \cdot \sqrt{\frac{T}{M}}$$

where *M* is the mass in amu and *T* is in degrees Kelvin. Here the units of Doppler width are the same units expressed as wavelength [5].

E. RIMS TECHNOLOGY SEQUENCE

A design intention of RIMS technology is to provide an alternative and more rapid method to analyze the isotopic composition of a certain material. RIMS technology is vastly less time consuming than other methods requiring chemical dissolution and separation treatments [6]. Once the sample is obtained, it is placed in the ionizing chamber and atomized into a gaseous cloud of both neutral and charged particles [5]. A timing sequence allows for these charged particles to be drawn out of the chamber by an applied voltage around 4000 V. The remaining cloud of material is, for the most part, neutral atoms and molecules. The set of three lasers (which are specifically tuned) are pulsed together to selectively ionize the cloud of neutrals of the targeted element (in our case plutonium) [5]. An additional applied voltage around 2000 V is triggered causing the resulting ions to be focused and travel into the drift region of a time-of-flight mass spectrometer for analysis [5]. The time of flight for each ion is determined by the ion's mass and can then be differentiated to determine the sample's isotopic composition [5]. This entire process can be completed in only a few hours and the modeling of RIMS will assist the technology by establishing a known benchmark of data for specific isotopes of interest.

III. MODELING PLUTONIUM FOR RIMS ANALYSIS

The purpose of the model is to analyze and predict the relative ionization probabilities of plutonium isotopes as they are excited using the three color, three photon pulsed laser irradiation. The model, when proven accurate, will provide a benchmark for the resonance ionization mass spectrometry of Pu and aid in understanding the sensitivity of isotope ratio measurements to laser system performance. Previous work using the model [7] did not incorporate the excitation and ionization cross sections for plutonium within the model, thus experimental data is needed to refine and complete the model for more complete analysis.

A. RATE EQUATIONS

The primary goal of the model is to calculate the population densities of four possible energy states in plutonium. The model framework uses an average laser excitation continuum to excite the neutral plutonium atoms to each specific energy level [6]. The four rate equations used to describe the rate of change in energy level populations are described in [6] as

$$\frac{dN_0}{dt} = W_{01}\left(N_1 - \frac{g_1}{g_0}N_0\right) + \frac{N_1}{\tau_1}$$

$$\frac{dN_1}{dt} = W_{01}\left(\frac{g_1}{g_0}N_0 - N_1\right) + W_{12}\left(N_2 - \frac{g_2}{g_1}N_1\right) - \frac{N_1}{\tau_1} + \frac{N_2}{\tau_2}$$

$$\frac{dN_2}{dt} = W_{12}\left(\frac{g_2}{g_1}N_1 - N_2\right) - \frac{N_2}{\tau_2} - W_{2ion}N_2 - W_{2C}N_2$$

$$\frac{dN_{ion}}{dt} = W_{2ion}N_2 + W_{2C}N_2$$

N_i is the number of atoms in state i, W_{ij} is the rate of transition from state i to j [6]. This is all assuming spontaneous decay occurs within this scheme of states and that radioactive decay is sufficiently long in duration compared to the laser induced excitation of the atoms. Additionally, a term like W_{2C} is added and subtracted where appropriate, to account for alternative ionization pathways into the continuum [6]. All atoms are also

assumed to be initially at their ground state energy in order to achieve consistency in the numerical results of the model.

The rates of transition are calculated from the atomic cross sections and the time-dependent spectral irradiances of the lasers and are given in [6] by

$$W_{ij} = \iint \sigma_{ij}(\lambda) I_i(\lambda, t) d\lambda dt$$

where $\sigma_{ij}(\lambda)$ is the transitional cross section between the respective states, and $I_i(\lambda,t)$ is the spectral irradiance of the laser for that given energy transition [6]. This rate is a function of the time-varying amplitude of the laser pulses, however, the time dependence is treated independently resulting in this equation from [6] that includes the time distribution of a pulse

$$W_{ij}(t) = W_{ij} T_i(t)$$

such that $T_i(t)$ is a Gaussian distribution given in [6] by

$$T_i(t) = \frac{1}{\sqrt{2\pi\sigma^2}} e^{\frac{-(t-T_0)^2}{2\sigma^2}}$$

where σ is the standard deviation of the pulse width and not the atomic cross section.

B. CROSS SECTIONS

The atomic absorption cross section, below, is defined in [6] as a function of wavelength to include the dipole matrix element $|D_{ij}|$ for a given transition and the normalized line shape $k(\lambda)$ of the transition. In addition, when dealing with specific substates the degeneracy factor is not included [6].

$$\sigma_{m_i m_j}(\lambda) = \frac{2\pi^2 k(\lambda)}{3\varepsilon_0 \hbar \lambda_0} | D_{ij} |^2$$

In this research, the modeling simulates the approximation of the transition cross sections for even-A isotopes. For this work, odd-A isotopes were treated as even isotopes for the purposes of the model assumptions, this work could be extended by including the

known complications of modeling odd-A isotopes as discussed in the literature [6]. Further research will be required to improve the model for odd isotopes.

For even-A isotopes, Isselhardt explains in [6], "the cross section as a function of wavelength is calculated as the product of the amplitude at the wavelength corresponding to the peak cross section and a normalized line shape"

$$\sigma_{ij}(\lambda) = \sigma_0 k(\lambda)$$

where σ_o refers to the peak cross section. Implementing the velocity distribution of the atoms in the ionization volume (assuming Maxwell-Boltzmann distribution) and the natural linewidth will result in a convolution of a Gaussian function with a Lorentzian function [6],

$$\sigma_{even}(\lambda) = \frac{\lambda_0^2}{4}\Gamma_{ji}\frac{g_j}{g_i}\left[D(\lambda) \otimes L(\lambda)\right]$$

where $D(\lambda)$ is the Doppler broadened line shape and $L(\lambda)$ is the Lorentzian pertaining to resonance natural linewidth [6].

Alternative methods for extracting ionization cross sections can be accomplished through experimental analysis of the saturation curves through RIMS. This has been conducted previously in [6] and [10] for uranium isotopes as two separate experiments using different methods with resulting cross sections of 1.67 x 10^{-15} cm^2 and 2.1 x 10^{-15} cm^2. In chapter IV, I will detail the experimental results and the extracted cross sections for Pu-239 and Pu-240. Anticipated results for ionization cross sections for plutonium should be on the same order of magnitude as uranium isotopic cross sections since the laser powers needed to saturate the transitions are in the same range of power. Below is the ionization population factor that represents the expected behavior from a saturation curve conducted via RIMS analysis. Within this equation from [10], the desired cross section for ionization is contained.

$$\frac{N_{ion}}{N_{ex}} = \left(1 - e^{\frac{-\sigma U}{2\hbar\omega A}}\right)$$

In addition to the cross section σ, the energy per pulse *U*, cross sectional area of the ionization volume *A*, and the energy per photon $\hbar\omega$ is used [10]. Table 2 lists the parameter inputs into this equation to construct the curve fits to the experimental data detailed in Chapter IV. The cross sectional area of the ionization volume was calculated by averaging the areas of two different radii measurements of the FWHM of the two-dimensional Gaussian laser profile.

Table 2. Excitation and Ionization Laser Parameters used for Data Analysis

	$\hbar\omega$ (Joules)	A (cm^2)
First Excitation Laser	4.73 E -19	0.0135
Second Excitation Laser	2.35 E -19	0.0151
Ionization Laser	2.59 E -19	0.0114

Finally, the autoionizing cross section can be derived as Isselhardt states in [6] "as a simple approximation as a discrete transition where the last photon absorbed excites the atom above the ionization limit, and then decays by ionization." This results in a full width of the autoionizing state written as

$$\Gamma = \Gamma_{\gamma\gamma} + \sum_{\gamma'} \Gamma_{\gamma\gamma'} + \Gamma_{e^-}$$

where $\Gamma_{\gamma\gamma}$ is the partial width of the autoionizing state, which decays back to the second excited state, $\Gamma_{\gamma\gamma'}$ is sum of other potential photon transitions, and lastly at the end is the partial width for electron emission [6]. Now when $E=E_0$ and neglecting Doppler broadening the cross section is written as

$$\sigma_{\gamma\gamma} = \frac{g_2}{g_1}\frac{\lambda_0^2}{2\pi}\frac{\Gamma_{\gamma\gamma}}{\Gamma}$$

where λ_0 is the transition wavelength [6].

C. LASER IRRADIANCE

Stability of the laser pulse distribution for nuclear forensic analysis using RIMS is of high importance. Fluctuations in laser distribution are the most limiting factors regarding the accuracy of RIMS [6]. Modeling these variations creates quite a challenge, such that in this research, our model uses a more practical approach with the time-independent spectral irradiance equation [11].

$$I_i(\lambda) = \phi_i l(\lambda)$$

This is the product of the normalized spectral distribution $l(\lambda)$ and the photon flux

$$\phi_i = (5\times10^9)\lambda_i P_i A$$

where P_i is the pulse intensity in micro-joules and A is the area of the laser beam in cm^2 [11]. This area is the same area listed in Table 2 and was directly placed into the model for comparison and analysis. The laser irradiance within the model takes laser cross sectional area and power inputs to determine the photon flux distributed to the simulated material. The correct mean wavelengths need to be used and the bandwidth of the laser wavelength between 5 and 15 picometers must be described properly to replicate the appropriate distribution across the isotopes of interest.

D. MODEL FUNCTIONALITY

A working model to simulate isotope ratios through RIMS analysis is only effective if the proper parameters are used in the model. The model assumes a temperature of 4000 K for the atoms, which is then used to estimate a Doppler broadening of the atomic cross sections as annotated in Table 3. Additional improvements to the model were implemented after the cross sections were iteratively determined from the curve fit of the experimental data detailed in Chapter IV. The cross sections were used to calculate Γ, the widths of the exciting and ionizing states, and are listed in Table 3.

Table 3. Isotope and Laser Specific Parameters for the Model

	Transition	$\Delta\lambda_D$ (nm)	Γ (nm)
^{239}Pu	First Excited State	0.00123	9.0 E -6
	Second Excited State	0.00248	5.1 E -8
	Auto Ionization	0.00225	2.6 E -7
^{240}Pu	First Excited State	0.00123	9.7 E -6
	Second Excited State	0.00248	6.7 E -8
	Auto Ionization	0.00225	2.1 E -7

Implementing key atomic data and refining the excitation and ionization cross sections for plutonium will help validate the use of LION-LLNL RIMS analysis of Pu for potential Department of Defense and nuclear forensics applications. Improving the accuracy of the model will allow greater confidence in the sensitivity of RIMS Pu measurements to laser system variation. This is demonstrated by the success of similar work in measurements of uranium isotope ratios (see $^{235}U/^{238}U$ ratio in Figure 7) that provided confidence that the available laser bandwidth and power were sufficient to produce reliable consistency of the results. Improvements to the modeling of Pu will help establish RIMS as a reliable source for nuclear forensic analysis of Pu.

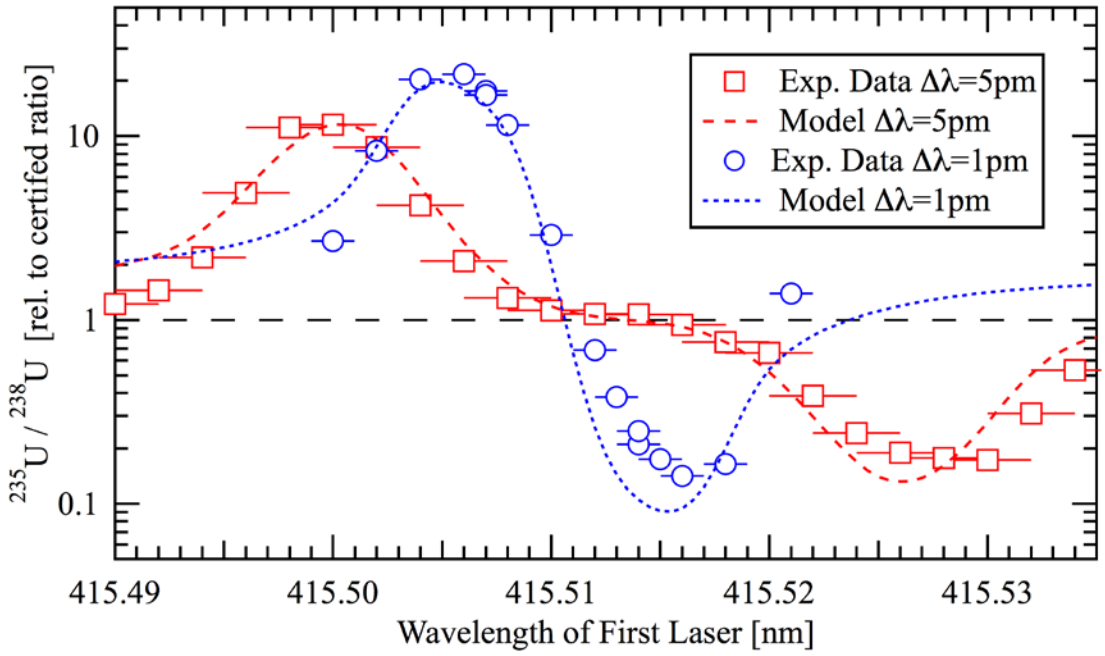

Figure 7. Measured and Predicted $^{235}U/^{238}U$ Ratio. Source: [6].

This work incorporates modifications to the model from previous work [7], by (1) integrating into the model the atomic parameters needed to determine the excitation and ionization cross sections for plutonium and (2) completing simulations with the resulting modified model in conjunction with experimental determination of parameters associated with saturation of energy transition processes. Specific improvements included calculations of the Doppler broadening, the widths of the excitation and ionization states, photon energies, and laser cross sectional areas. Additional adjustments included defining the centroid of the resonances that corresponded to the transition wavelengths for each plutonium isotope. With these adjustments, the framework is now set for modeling additional isotopes of interest such as americium (Am) and neptunium (Np). Detailed atomic parameters for Am and Np are documented in the appendix. The model now has the capability of providing accurate simulations of plutonium ionization. It can now use the atomic data and predict the cross sections for each isotope of plutonium as seen in Figure 8. The challenge of measuring Pu isotopes by RIMS is noted in Figure 8, showing the difference in wavelengths for the first energy transition between the two isotopes of about three picometers. Thus, the precision required in laser wavelength and linewidth

highlights the importance of experimental data for improving the fidelity of model predictions.

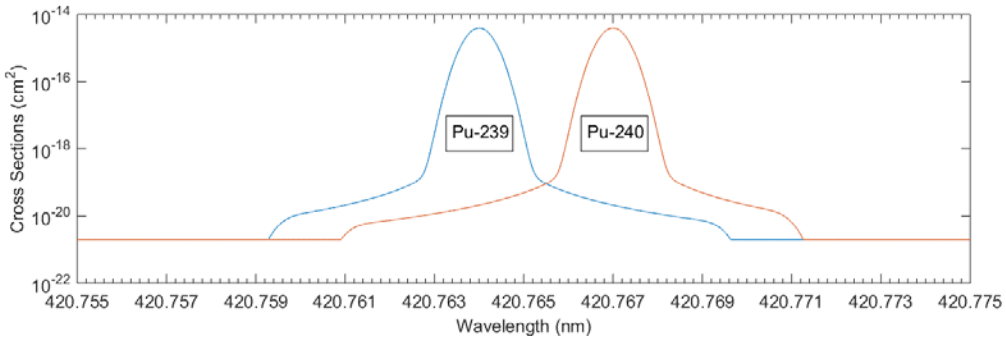

Figure 8. Cross Section (First Laser) vs. Wavelength

IV. EXPERIMENT AND MODEL RESULTS

In the effort to improve the accuracy of the model, an experiment was conducted using RIMS on a sample containing plutonium. This experiment is required to empirically derive the excitation and ionization cross sections for the isotopes of plutonium. These cross sections are then implemented within the model and compared to the experimental data to determine if the saturation curve satisfies its expected trend. The experiment also confirms that specific laser parameters used in the model agree with the actual values, such that the expected ionization probabilities predicted by the model and described in literature agree.

A. EXPERIMENT

The experiment was conducted at LLNL using the LION-RIMS system. LION uses three tunable titanium doped sapphire laser cavities in order to achieve the desired laser parameters for saturating the ionization of plutonium. Critical laser parameters include mean wavelength, bandwidth, irradiance, relative timing and spatial distribution all of which allow for optimization of the RIMS performance [6]. The LION system uses time-of-flight mass spectroscopy to differentiate between the various isotopes of the element that is ionized. Upon ionization, a voltage of 2000 V is applied to the chamber causing the ions from the plutonium sample to travel into the drift region of the mass spectrometer. The difference in time of arrival at the detector is characteristic of the isotope mass, where heavier ions will take longer to reach the detector.

In this experiment, LION-RIMS uses three different pulse lasers to induce the electron transitions in the plutonium isotopes until the atoms are resonantly ionized. Table 4 lists the centroid of the resonance wavelengths for each isotope's electronic transition. During the experiment, two of the three lasers maintained a constant power, while the third laser's power varied. This varying of power was accomplished manually after each measurement. Figure 9 shows the three-pulsed lasers setup at the LLNL-LION facility.

Table 4. Wavelengths for Energy State Transitions in Pu. Adapted from [9].

Isotope	**λ_1 (nm) E_g to E_1**	**λ_2 (nm) E_1 to E_2**	**λ_3 (nm) E_2 to E_{ion}**
^{238}Pu	420.762	847.280	767.530
^{239}Pu	420.764	847.274	767.530
^{240}Pu	420.766	847.269	767.530
^{241}Pu	420.767	847.268	767.530
^{242}Pu	420.770	847.271	767.530

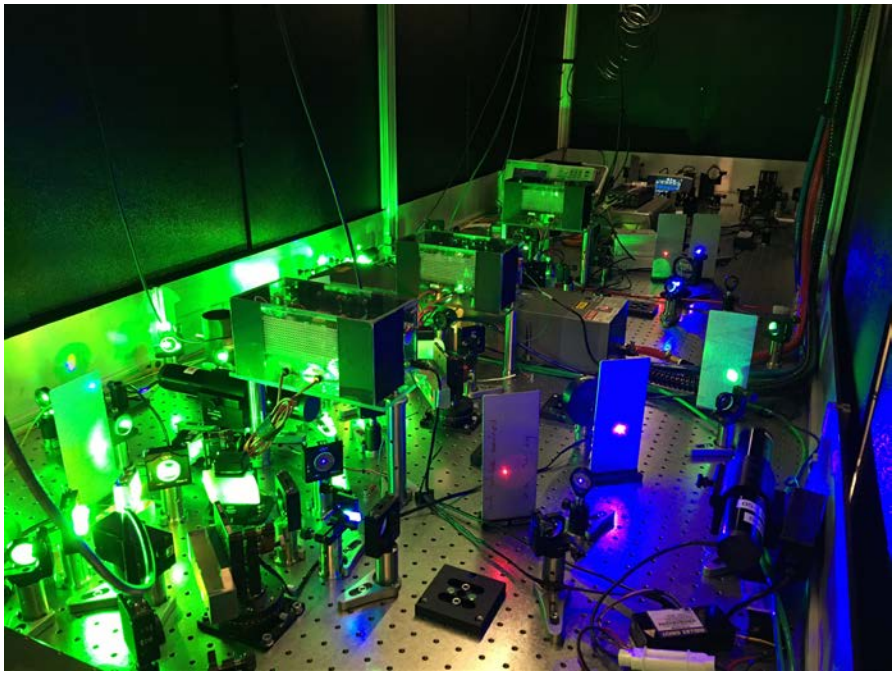

Figure 9. RIMS Three Tunable Lasers at LLNL-LION Facility

The first test maintained laser 2 at 1300 mW power and laser 3 at 1200 mW power, while incrementing laser 1 from 0-120 mW. Counts for each isotope during each test were tabulated for data analysis. The second test maintained laser 1 at 95 mW and laser 3 at 1200 mW, while varying laser 2 from 35-1090 mW. The final test maintained laser 1 at 95 mW and laser 2 at 1300 mW, while varying laser 3 from 6-860 mW. The counts were normalized by the maximum number of counts in each isotope order to form saturation curves, where 1 represents all available atoms have been ionized. The value for

the maximum number of counts was determined by taking the average counts of the data points that appear to have reached complete saturation. These experimental plots are essential to characterize important parameters of each laser and to determine each plutonium isotope's cross section for incorporation into the RIMS model. The following data tables show the total ion counts from RIMS measurements of the plutonium sample for the five isotopes detected. Table 5 consists of the data extracted from varying the power in the laser used to excite the first transition. Table 6 contains the data extracted from varying the output power in the laser used to excite the second transition. Finally, Table 7 details the data extracted from varying the power in the laser used to ionize the atom from the second excited state. Laser powers were varied in a random order to account for any change in the atomization rate of the sample over the course of an experiment.

Table 5. Plutonium Isotope Counts when Varying the First Laser

Power (mW)	^{238}Pu	^{239}Pu	^{240}Pu	^{241}Pu	^{242}Pu
120	258	84889	20731	613	1325
78	246	83021	20303	573	1203
42	249	81470	19624	590	1255
18	245	75842	18316	517	1085
9	227	78326	18488	550	1144
78	228	75538	18093	534	1215
3	188	70965	16747	524	998
58	249	73514	17847	514	1121

Table 6. Plutonium Isotope Counts when Varying the Second Laser

Power (mW)	^{238}Pu	^{239}Pu	^{240}Pu	^{241}Pu	^{242}Pu
1090	163	50574	11963	351	763
745	179	52178	12402	408	825
365	164	53541	12778	363	806
120	109	36304	8225	277	528
50	77	25504	5896	162	407
195	166	54676	12859	393	789
35	59	20407	4717	158	298
215	171	54827	12917	357	825
170	156	49641	11774	332	775
275	167	55127	13238	382	853
905	170	60601	14305	459	922
623	164	57190	13701	423	837

Table 7. Plutonium Isotope Counts when Varying the Third Laser

Power (mW)	^{238}Pu	^{239}Pu	^{240}Pu	^{241}Pu	^{242}Pu
500	112	36306	8901	258	531
200	100	34839	8256	239	485
860	103	34811	8398	264	522
380	105	33969	8146	228	497
55	85	29611	6900	187	393
10	44	15533	3444	89	109
79	84	28717	6738	179	331
29	78	23493	5540	134	245
6	16	7371	1653	46	38
45	73	25743	6157	182	304

There is strong correlation between the counts of ^{239}Pu and ^{240}Pu during all three of these measurements and is expected since ^{239}Pu and ^{240}Pu are the primary constituents that make up the plutonium sample. The other, less abundant isotopes, show more variation because the small number of counts results in large statistical variations. Additionally, the time of flight mass spectrometer was able to distinguish plutonium oxide compounds from the specific atomic plutonium isotopes tabulated above.

B. MODEL SETUP

The model can be arranged to produce either saturation curves or isotope ratio sensitivity analysis curves. Previous plutonium isotope ratio analysis has been conducted in [7] and detailed the effect varying bandwidth had on the model's accuracy. Saturation curve analysis for ^{239}Pu and ^{240}Pu were modeled for comparison to experimental results. An iterative method was used to determine the excitation and ionization cross sections.

The model is designed to use a specific function built using atomic data to export the desired cross sections, however, the function output displayed erroneous data during the troubleshooting process and was not used. In this analysis, the automatic cross section outputs were bypassed by inputting the estimated cross sections into the rate equation model and determining best fit through an iterative process. The cross sections were expected to be close to the cross sections of uranium around the magnitude of 10^{-16} cm^2 as the laser parameters used for ionization are comparable between the two elements [6]. This provided a reasonable starting point for iterative analysis in order to achieve the proper fit to the saturation curves for plutonium excitation.

C. EXPERIMENT AND MODEL COMPARISON

The experimental data points were normalized based on the average of the four highest data counts and the results were plotted in MATLAB. An iterative fit curve was used on these data points and the cross sections extracted by plotting the following equation from [10] into the curve fit analysis:

$$\frac{N_{ion}}{N_{ex}} = \left(1 - e^{\frac{-\sigma U}{2\hbar\omega A}}\right)$$

After the curve fitting was complete, the ionization probability model was executed and the results were overlaid with the experiment data points. Again, the cross sections were determined by trial and error based on the best curve fit that appeared nearest to the experimental data points. This method was performed for each varying laser and for both Pu-239 and Pu-240. Figure 10 and Figure 11 show the saturation curves when varying power in the first laser for Pu-239 and Pu-240, respectively.

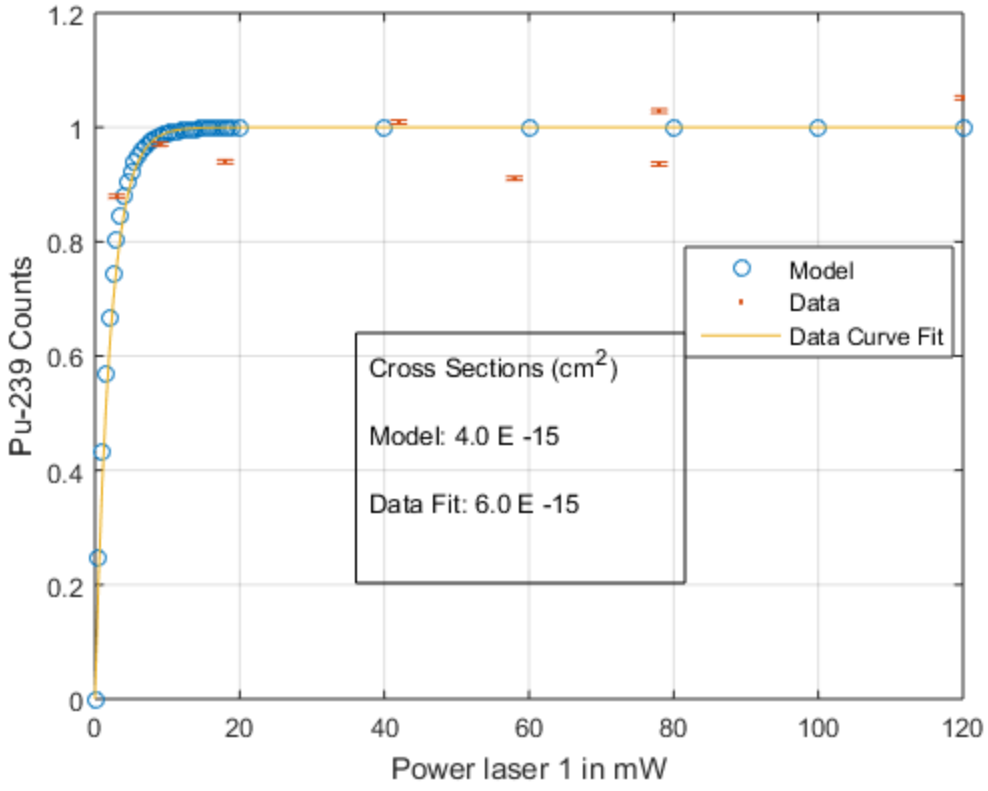

Figure 10. Pu-239 Saturation Curve, Varying Power in Laser 1

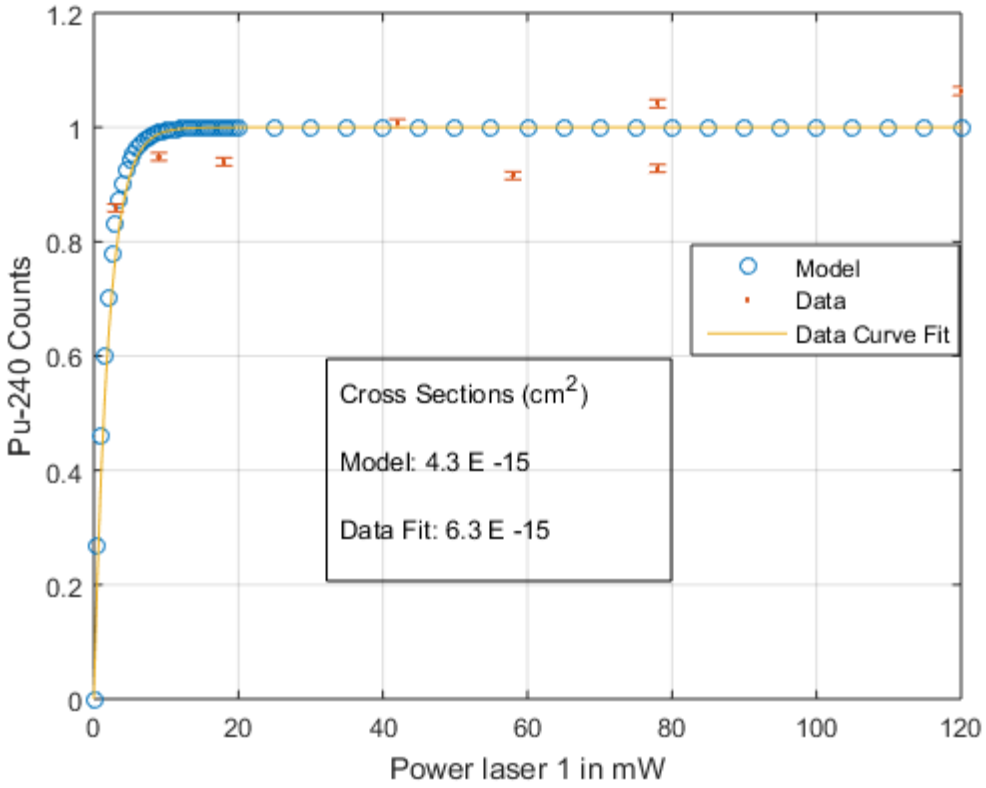

Figure 11. Pu-240 Saturation Curve, Varying Power in Laser 1

The data obtained displays a sharp increase in counts at very low powers. This rapid increase on the data curve implies that the cross section is larger than anticipated. This rise is a result of only two data points correlating to the curve fit, whereas the rest of the data points achieved saturation. This creates a large uncertainty on the fit of the data, which can be proven by performing the experiment again with a larger beam area to reduce the local laser beam irradiance and provide a slower rise in excitation probability. The resulting sum of squares difference for the fit of the experimental data is 0.0345 for Pu-239 and 0.0307 for Pu-240.

Figure 12 and Figure 13 show the saturation curves when varying power in the second laser for Pu-239 and Pu-240, respectively. The curve fit for the experimental data trended as expected, and in this case, there is only a small fraction of difference between cross sections. This shows solid agreement between the model predictions and the fit to the experimental data. The sum of squares difference for the data curve fit was 0.1905 for Pu-239 and 0.1297 for Pu-240.

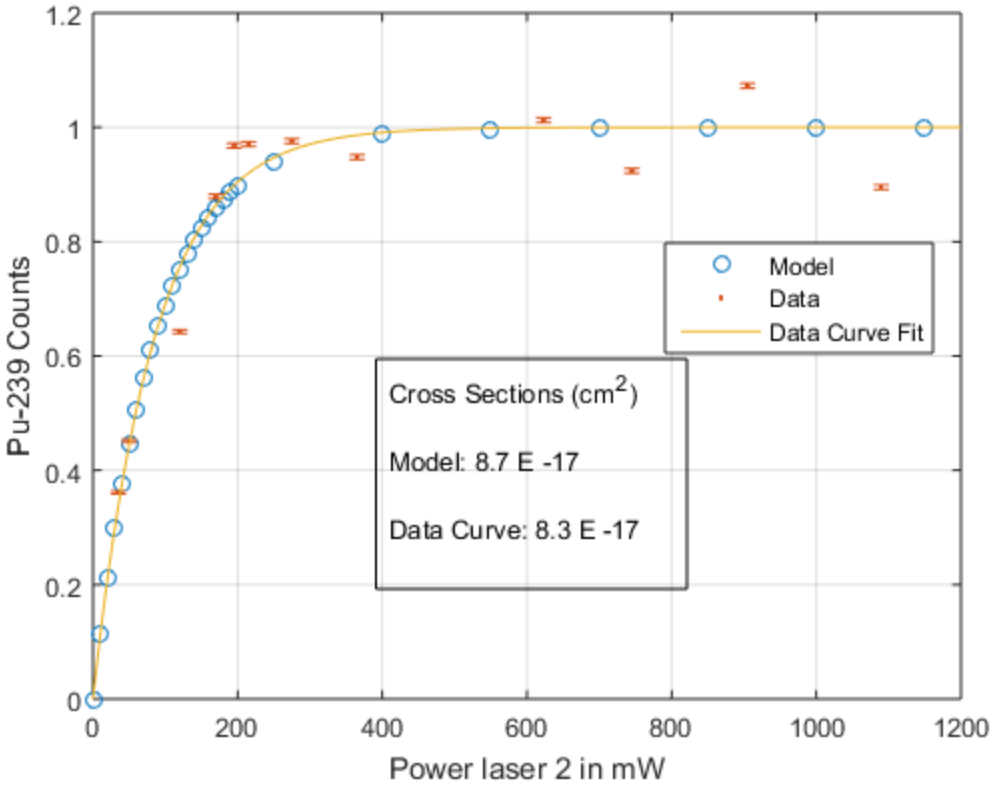

Figure 12. Pu-239 Saturation Curve, Varying Power in Laser 2

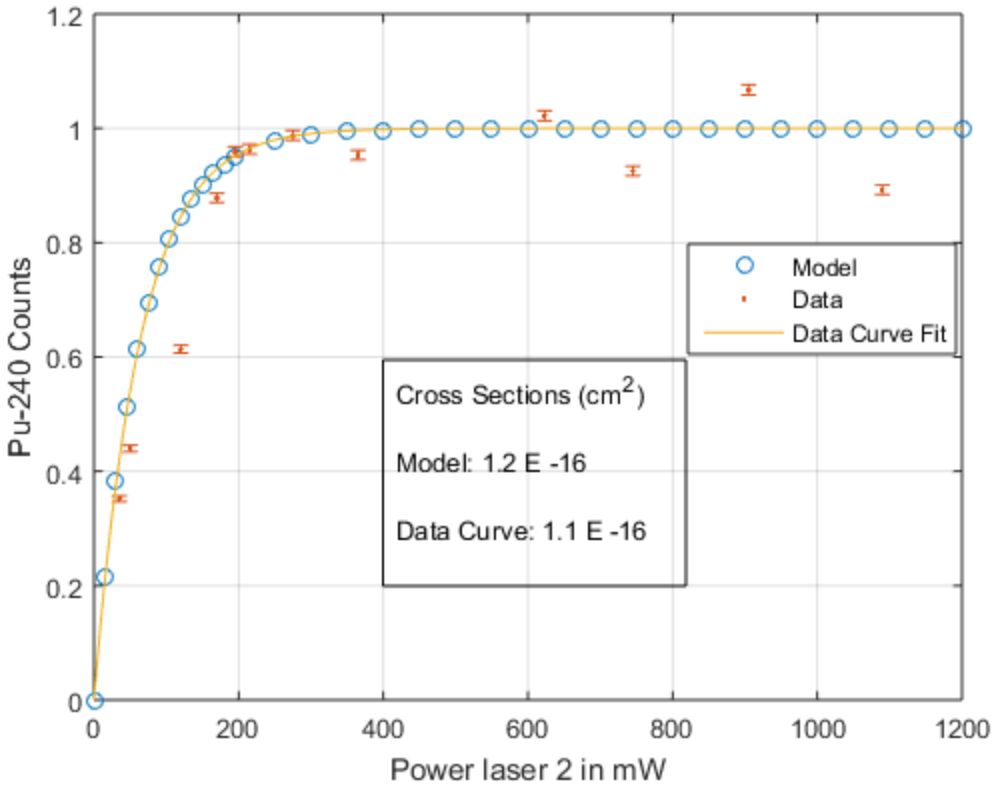

Figure 13. Pu-240 Saturation Curve, Varying Power in Laser 2

Figure 14 and Figure 15 show the saturation curves when varying power in the third laser for Pu-239 and Pu-240, respectively. Both curves demonstrate the expected non-linear trend and are situated on the plot in identical locations. Similar to the Figure 12 and Figure 13 with varying the power in laser 2, the cross sections are on the same order of magnitude and the data curve fit has a smaller cross section than the model. The sum of squares difference for the experimental data least squares curve fit was 0.2159 for Pu-239 and 0.2115 for Pu-240.

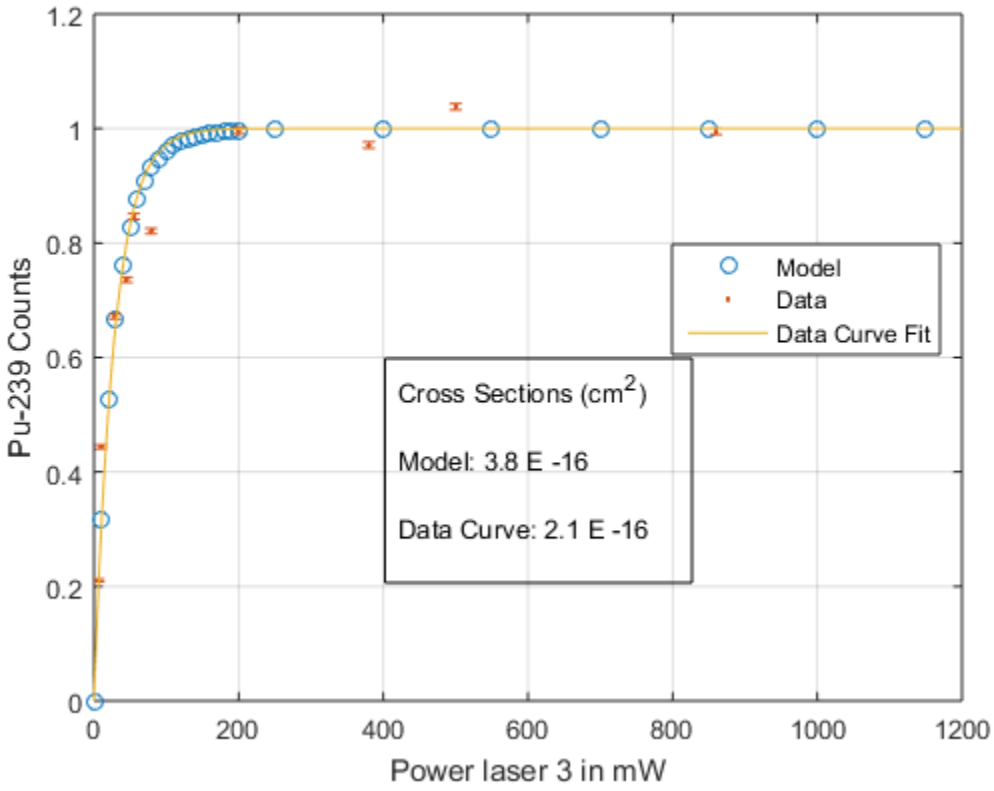

Figure 14. Pu-239 Saturation Curve, Varying Power in Laser 3

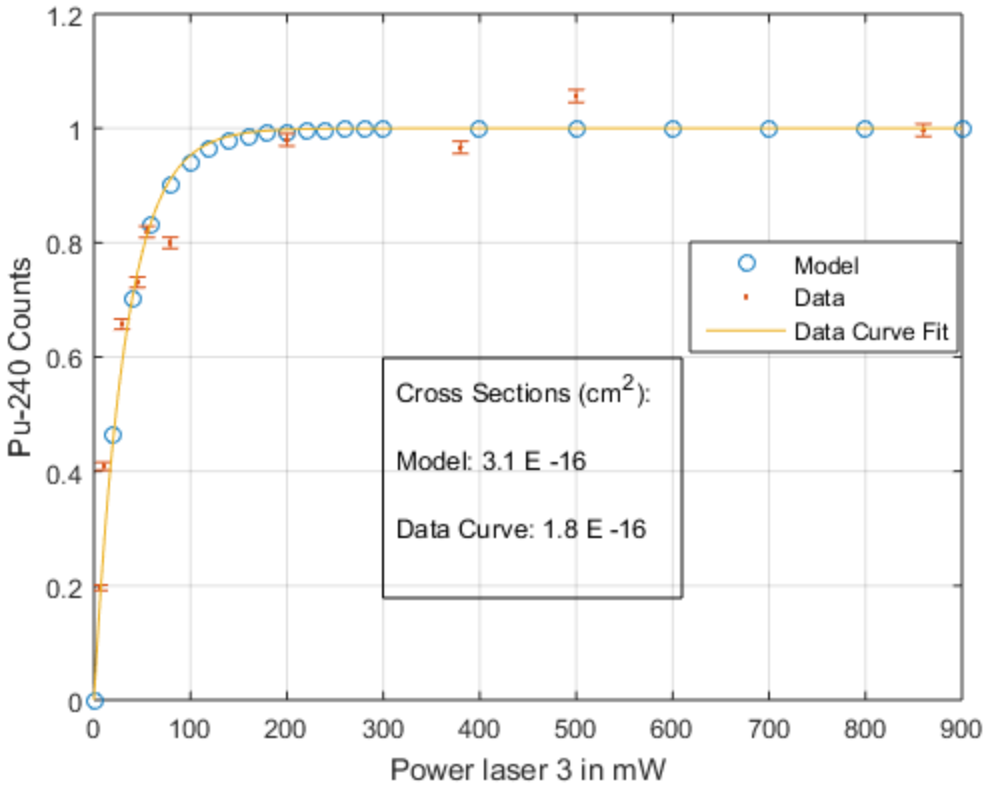

Figure 15. Pu-240 Saturation Curve, Varying Power in Laser 3

With these cross sections estimated, we can now study the sensitivity of Pu to the variations in the laser parameters. Additionally, we can model the ratio of the ionization probability of different Pu isotopes. Figure 16 shows the predicted Pu-239/Pu-240 ratio as a function of wavelength of the first of three excitation lasers. This precision in distinction between isotopes allows us to further refine the model in order to accurately predict the parameters needed for an actual RIMS analysis. The model allows for countless data simulations in order to predict isotope behavior, rather than conducting multiple time intensive data collections with RIMS experiments.

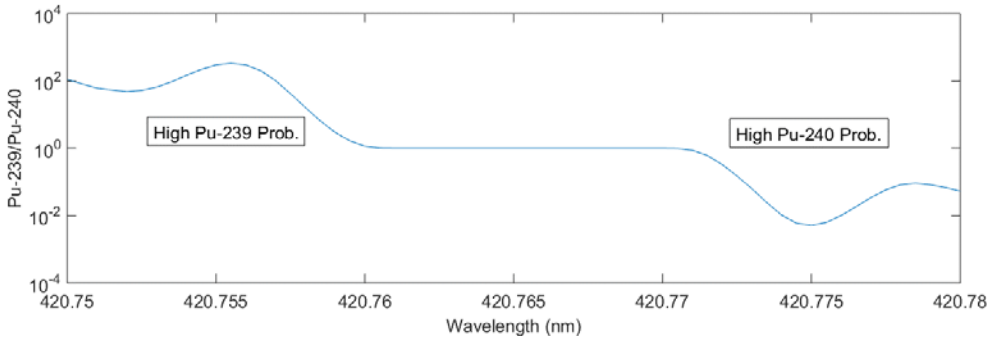

Figure 16. Predicted $^{239}Pu/^{240}Pu$ Ratio as a Function of Wavelength (First Laser)

D. SUMMARY

All three experiments showed the cross sections to be on the same order of magnitude and near the anticipated values upon comparison between experimental results and model simulation. A potential contribution to errors in the experiment is that the experiment uses finite material and number of atoms, whereas the model simulation is simply a point model. The experiment runs out of atoms in the center of the cloud and the model does not account for the spatial effect. This difference contributes to the model cross sections to be slightly higher than the experiment cross sections. The only exception to this was for the first laser where further data collection is required with a larger laser beam area. The resultant cross sections for ionization that the model predicted and the experiment estimated are near the values expected from previous work [6] conducted on uranium with RIMS. These cross sections can now be used in the model to study the sensitivity of Pu measurements by RIMS to variations or differences in the laser characteristics during experiments.

THIS PAGE INTENTIONALLY LEFT BLANK

V. CONCLUSION

For the past seven decades, the world has understood the devastating effects from the detonation of a nuclear device. Advancements in nuclear forensics through the use of RIMS will help expedite the process for analyzing interdicted special nuclear material. These advancements are critical in order to prevent nuclear material from being available to adversary countries or terrorist organizations. On September 9, 2016, North Korea conducted its fifth nuclear test and has claimed the capability of mounting a nuclear warhead on a ballistic missile [12]. North Korea's unpredictable posture, ability to conduct nuclear testing, and capability of long range ballistic missile testing highlights the importance for rapid nuclear forensic analysis techniques such as RIMS.

A. SUMMARY

The research incorporated existing and experimental data of plutonium isotopes in nuclear materials into the simulation model framework for RIMS. Through model simulation and curve fitting of experimental data, we were able to obtain estimated values for the excitation and ionization cross sections of plutonium. Although the cross sections differed slightly between the fits of experimental data and the model, this analysis provides the necessary data to improve the modeling of Pu relative ionization probability. Both the model and the experimental data points replicated the predicted saturation curves as shown in Figures 10-15. Additional experimental data with a larger laser beam area for laser 1, would provide more precise estimates of the first cross section. Refining the model parameters, to include odd-A isotope effects, as described in [5], will be essential for improving the accuracy of the model predictions for odd-A isotopes. Additionally, improving the model to replicate the spatial dependence of the experiments will minimize the difference between model and experimental results. The use of a reliable and predictable model of RIMS for nuclear forensic analysis is vital to help define the performance of RIMS to characterize isotope ratios in retrieved samples from a detonated nuclear device.

B. FUTURE RESEARCH

The outcome of this research opened up several opportunities to advance the field of RIMS technology. As mentioned previously, further experimental analysis of plutonium with RIMS is needed in order to refine the cross sections to better agree with model predictions. Expansion of the model is needed to include more elements of the actinide series such as americium (Am) and neptunium (Np), which are formed as decay products from Pu and U [13]. Some studies already exist for Am and Np and their key parameters are available in the literature; however, no comparisons of a predictive model and experimental RIMS results have been reported for these elements [14–18].

Ongoing work is being conducted to substitute the second pulsed laser from the LLNL-LION system and replace it with a continuous wave laser [19]. This will be beneficial to compare our known pulse laser experimental data with the new continuous wave laser results. Modeling the continuous wave laser for plutonium is also possible since there are already sufficient descriptions of the laser beams in the literature [20]. Further engineering research can be utilized to mobilize the RIMS system for practical field use. Designing a transportable unit for the Department of Defense for field use can minimize the delay in the delivery of results to key decision makers.

APPENDIX. NEPTUNIUM AND AMERICIUM DATA

Future research requires the model to incorporate additional actinides such as Np and Am. These two elements are the byproducts of the spent nuclear reactor fuel and decay of uranium and plutonium [13]. Np-237 has an extremely long half-life ($t_{1/2}$ = 2.14 million years) and can expose a hazard to the environment since it is easily soluble in water [16]. Am-241 is a decay product of Pu-241, such that an accurate RIMS analysis of Am-241 would complement the nuclear forensic efforts [13].

A. NEPTUNIUM-237

Np-237 is produced in a reactor through neutron irradiation of uranium or plutonium [13]. The desired atomic parameters are the same as those used in plutonium in order to confirm the validity of RIMS through model simulations. Future excitation and ionization data of Np-237 will be required to empirically derive the cross sections. The neutron spin for Np-237 is $I = 5/2$ and the Doppler broadening is 0.15 cm^{-1}. Additional parameters proven effective with RIMS are listed in Table 8.

Table 8. Atomic Parameters of Np-237 for RIMS model.
Adapted from [16].

	λ (nm)	*J*	Energy (cm^{-1})	Sat. Power (mW)
First Laser	380.74	11/2	26264.37	6.6
Second Laser	794.93	9/2 – 11/2	38843.95	33
Third Laser	812.82	7/2 -13/2	51146.5	≥ 500

B. AMERICIUM-241

There is very little literature regarding the use of RIMS on americium, which makes future experiments with LION-LLNL on americium quite challenging. There is, however, a great deal of atomic structure data on americium as detailed in [14] and [17]. Am-241 has a nuclear spin of $I = 5/2$ and an ionization energy of 48,182 cm^{-1} [14]. Its half-life is 432 years and is the product of decay from Pu-241. Specific laser parameters needed for excitation and ionization for the use with RIMS still need to be determined.

LIST OF REFERENCES

[1] R. Rhodes, *The Making of the Atomic Bomb*. New York, NY: Simon & Schuster August 1, 1995.

[2] S. Glasstone and P. J. Dolan, *The Effects of Nuclear Weapons*, Third Edition, Washington, DC, United States Atomic Energy Commission, 1977.

[3] F. G. Gosling, *The Manhattan Project: Making the Atomic Bomb*. United States Department of Energy, Washington, DC, DOE/MA-0002, 1999.

[4] K. Mayer et al., "Nuclear forensic science-from cradle to maturity," *J. of Alloys and Compounds*, vols. 444–445, Oct. 2007, pp. 50–56.

[5] B. H. Isselhardt, "Quantifying uranium isotope ratios using resonance ionization mass spectrometry: The influence of laser parameters on relative ionization probability," Ph.D. dissertation, Dept. Eng., Univ. California, Berkeley, 2011.

[6] B. Isselhardt, S. Prussin, M. Savina, D. Willingham, K. Knight and I. Hutcheon, "Rate equation model of laser induced bias in uranium isotope ratios measured by resonance ionization mass spectrometry," *J. Anal. at. Spectrom.*, vol. 31, pp. 666–678, 2016.

[7] C. T. Lensegrav, "Advanced quantification of plutonium ionization potential to support nuclear forensic evaluations by resonance ionization mass spectrometry," M.S. thesis, Dept. Physics, Naval Postgraduate School, Monterey, CA, 2015.

[8] K. Wendt, N. Trautmann, "Recent developments in isotope ratio measurements by resonant ionization mass spectrometry," *Int. J. of Mass Spectrometry*, no. 242, pp. 161–168, 2005.

[9] S. Raeder, "Trace analysis of actinides in the environment by means of resonance ionization mass spectrometry," Ph. D. dissertation, Inst. for Physics, University of Mainz, 2010.

[10] D. Willingham, M. R. Savina, K. B. Knight, M. J. Pellin and I. D. Hutcheon, "RIMS analysis of ion induced fragmentation of molecules sputtered from an enriched U3O8 matrix," *J. Radioanal. Nucl*., vol. 296, pp. 407–412, 2013.

[11] M.G. Hurst and G.S. Payne, *Principles and Applications of Resonance IonizationSpectroscopy*. London: CRC Press, 1988.

[12] J. Rosen, J. Wachtel, C. Pergram. (2016, September 9). World condemns North Korea's 'biggest' nuclear test. *Fox News World* [Online]. Available: www.foxnews.com/world/2016/09/09/seoul-says-north-korea-conducted-5th-nuclear-test.html

[13] K. B. Knight *et al*., "Prioritization study of elements relevant to RIMS counter-WMD," LLNL, Livermore, CA, TR-652515, Mar. 2014.

[14] V. Fivet *et al*., "Transition probabilities in complex ions: the case for americium." *Journal of Electron Spectroscopy and Related Phenomena*, vol. 156–158, pp. 255–258, 2007.

[15] J. Riegel *et al*., "Resonance Ionization Mass Spectrometry for trace analysis of neptunium." *Applied Physics B: Photophysics and Laser Chemistry.* vol. 56, pp. 275–280, Feb 1993.

[16] S. Raeder *et al.*, "Determination of the 3 step excitation and ionization scheme of 237-Np for trace analysis of RIMS." *Spectrochimica Acta part B: Atomic Spectroscopy.* vol. 66, no. 3–4, pp. 242-247, Mar.–Apr. 2011.

[17] R. Deissenberger *et al.*, "First determination of the ionization potential of americium and curium." *Angewande Chemie International Edition in English.* vol. 34, no. 7, pp. 814–815, Apr. 1995.

[18] S. Kohler *et al.*, "Determination of the first ionization potential of actinide elements by resonance ionization mass spectrometry." *Spectrochimica Acta part B: Atomic Spectroscopy.* vol. 52, no. 6, pp. 717–726, Jun 1997.

[19] S. G. Lau, "Characterization of a continuous wave laser for resonance ionization mass spectroscopy analysis in nuclear forensics," M. S. thesis, Dept. Physics, Naval Postgraduate School, Monterey, CA, 2015.

[20] P. Kunz *et al.*, "Resonance ionization mass spectrometry (RIMS) with pulsed and CW-lasers on plutonium." *Hyperfine Interactions,* vol. 162, pp. 159–166, 2005.

INITIAL DISTRIBUTION LIST

1. Defense Technical Information Center
   Ft. Belvoir, Virginia

2. Dudley Knox Library
   Naval Postgraduate School
   Monterey, California